JOURNAL OF AIRCRAFT
Vol. 29, No. 2, March–April 1992

Effects of Ambient Turbulence on the Decay of a Trailing Vortex Wake

H.-T. Liu*
QUEST Integrated, Inc., Kent, Washington 98032

Experiments were conducted to investigate the effects of ambient turbulence on the evolution of a trailing vortex wake. The wake was generated by towing an NACA 0012 wing, with a span of 10.2 cm and a chord of 5.1 cm, at an incidence of −10 deg and a speed of 40 cm/s in a tow tank. The chord Reynolds number was 20,400. The ambient turbulence was generated by towing three grids, with square meshes of 1.45, 10.2, and 20.3 cm, upstream of the wing. Turbulence parameters were measured with crossed hot-film probes. The trailing vortex wake, tagged with a fluorescent dye, was visualized from different perspectives and its decay was derived from 16-mm movie records. For weak turbulence with large integral scales compared with the vortex separation, vortex linking is the dominant mode of instability. The dominant wavelength of the linking decreases with increasing turbulence intensity or dissipation rate. As the turbulence intensity increases, vortex bursting appears and eventually replaces linking as the dominant mode of instability. For turbulence with a small integral scale as compared with the vortex separation, vortex instability is predominantly of the bursting type.

I. Introduction

THE ever-increasing demand in air transportation capacity has led to serious congestion in many airports. Because aircraft spacing is largely dictated by the characteristics of the vortex wakes left by aircraft, an in-depth understanding of the mechanisms that bring about wake dissipation would provide information to determine the optimum aircraft spacing.

Studies have demonstrated that atmospheric disturbances such as stratification, windshear, and turbulence have a strong influence on the evolution of aircraft vortices.[1-3] However, systematic investigation of these processes is hampered by difficulties in controlling the test conditions and in collecting quantitative results during full-scale flight tests. On the other hand, wind-tunnel testing is limited for studying the wake evolution process because the vortex wake is quickly swept downwind of the working section. Although empirical, analytical, and numerical models have been developed to investigate the vortex wake phenomenon, these models have not been subjected to thorough verification due to the lack of quantitative field or laboratory data.[2-6] An operational analytical/numerical model that takes into consideration all the important atmospheric disturbances does not currently exist.

The use of a tow tank has been demonstrated to be most suitable for studying the evolution of vortex wakes.[7] The simulated vortex phenomenon has the same spatial and temporal references as that of airplanes, and ground effects on the vortex evolution may be easily simulated under different atmospheric conditions. Tow tank experiments have been conducted to study various devices for the attenuation of vortex wakes,[8] the swirl motion in vortex wakes,[9] and the effects of stratification on the rise of vortices.[10,11] The results of such tests help to improve our understanding of these effects on vortex wake behavior and provide bench data for the validation of analytical/numerical models.

This paper describes experiments conducted in a tow tank at QUEST Integrated, Inc., to study the effects of ambient turbulence on the evolution of vortex wakes.

Received Nov. 13, 1990; revision received March 30, 1991; accepted for publication April 10, 1991.

*Principal Scientist, Applied Physics Division, QUEST Integrated, Inc. (formerly Flow Research, Inc.), 21414-68th Avenue South. Member AIAA.

II. Background

As soon as a vortex wake is formed, the aging process begins as a consequence of turbulence diffusion, entrainment, and dissipation. In a quiescent background, deintensification of vortex pairing results from sinusoidal instability[12] and from vortex breakdown.[13,14]

Sinusoidal instability is a convective instability that arises by balancing the self-induced rotation of a sinusoidally deformed vortex with the velocity induced at this vortex by the deformed opposite vortex.[12] The amplification rate of the instability is exponential in time and depends on the vortex core structure.[15] As a result of the sinusoidal instability, linking of the two trailing vortices occurs at the position of minimum separation and leads to the formation of a series of vortex rings. Figure 1 is a series of still photographs (top view) showing the development of the sinusoidal instability of a trailing vortex pair generated by a wing towed in a tank of quiescent water.

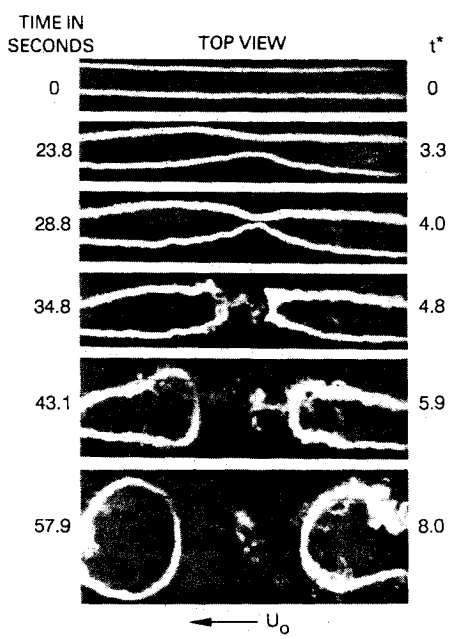

Fig. 1 Development of a sinusoidal instability of a trailing vortex pair generated by a towed NACA 0012 wing in a quiescent environment.

Vortex breakdown or bursting may be described as the abrupt structural change of the tube of a vortex that is precipitated in a smooth flow seemingly for no reason. The exact cause of vortex breakdown is not yet thoroughly understood, although simplified theories have been developed in an attempt to explain the breakdown phenomenon.[16] Vortex breakdown manifests itself as a localized bursting phenomenon, or a sudden increase in the diameter of a single vortex core, and often results in a very turbulent flow.

In a turbulent environment, the aging of vortex wakes becomes a complicated process. Several investigators have studied the effects of ambient turbulence through numerical simulation. Bilanin et al.[3] studied numerically the dissipation of a two-dimensional vortex wake in the presence of ambient turbulence. A second-order closure model was used to represent the turbulence. However, this two-dimensional model is incapable of addressing the behavior of sinusoidal instability and of vortex bursting because these phenomena are inherently three-dimensional. The numerical results show that the circulation drop-off as a function of time changes from $t^{-1/2}$ with no ambient turbulence to t^{-2} with turbulence.

Assuming that the integral scale of the ambient turbulence is large compared with the vortex separation, Crow and Bate[2] derived the following expression to predict the lifespan of a trailing vortex pair or the time at which the two vortices touch due to linking instability:

$$t_l^{*1/4} e^{-0.83 t^*} = 1.15\varepsilon^*, \qquad \varepsilon^* < 0.3 \tag{1a}$$

$$t_l^* = 0.41\varepsilon^{*-1}, \qquad \varepsilon^* > 0.3 \tag{1b}$$

where $\varepsilon^* = (\varepsilon b_0/W_0^3)^{1/3}$ and $t_l^* = W_0 t_l/b_0$. Here, b_0 is the vortex separation, t_l is the lifespan, W_0 is the initial vortex downwash velocity, and ε is the turbulence dissipation rate. The two parts of Eq. (1) are matched at $\varepsilon^* = 0.3$.

Using a light Cessna 170 airplane with a wingspan of about 11 m, Tombach[1] conducted a series of experiments in the atmospheric boundary layer under a wide range of stability conditions. He estimated the lifespan of the vortex pair from the visual records and found that the data may be enveloped by two lines

$$t = 15\varepsilon^{-1/3} \tag{2a}$$

$$t = 70\varepsilon^{-1/3} \tag{2b}$$

where t is the time. For the cases where linking of the vortex pair was observed, the lifespan agrees fairly well with the predictions of Crow and Bate,[2] i.e., Eq. (1). One finding of particular interest is that at any level of turbulence the lifespan tends to be the same, regardless of whether the instability is bursting or linking. This suggests that, at least to first order, $\varepsilon^* = (\varepsilon b_0/W_0^3)^{1/3}$ may be the only dimensionless parameter required to determine the effects of ambient turbulence on the lifespan of vortex wakes. For isotropic turbulence,[17] the following relationship holds:

$$\varepsilon = Kq^2/L_f \quad \text{with} \quad K = 0.25 \tag{3}$$

where q^2 is the total turbulence kinetic energy and L_f is the integral scale of the turbulence. If Eq. (3) is proven sufficient to specify the ambient turbulence, all we need to measure is q^2. Note that the ground effects, with the length scale of atmospheric turbulence proportional to the height above ground, have not been incorporated in Eq. (3).

III. Experimental Approach and Methods

Tow Tank

The tow tank is 18.3 m long, 1.2 m wide, and 0.91 m high and has glass sidewalls and floor to permit visualization from all directions. The tank may be filled with either fresh water or salt water of varying salinity to simulate a variety of atmospheric and oceanographic conditions. A model can be towed at a uniform velocity or in a controlled, cyclic acceleration/deceleration mode. The towing system includes two sets of towing cables, driving pulleys, drive shafts, motors, and controllers. A slotwheel with 16 slots is attached to the drive shaft of each motor, and a light emitter/photosensor combination is used to measure the towing speed. The tow tank facility has several special features:

1) The tow tank is equipped with tow carriages. The shoes of the carriages ride two straight tracks, one flat and one round, on a thin film of oil to ensure smooth towing operations. The noise level, due to vibration and nonuniformity of the tow speed, as measured with a hot-film probe towed in a quiescent fluid, is less than 0.3% of the towing speed. This does not represent the ambient turbulence in the same sense as that in a wind tunnel. The fluid in the tank is indeed quiescent provided there is no noticeable temperature difference between the room air and the water.

2) A special mounting method is used for wing and airplane models, replacing the undesirable strut or sting method with three thin stainless-steel wires from which the model is hung. This system is very stable except in an extremely turbulent environment.

3) The tow tank is equipped for conducting flow visualization experiments using dyes illuminated by conventional and laser light sources, as well as quantitative measurements of flow properties using hot-film and conductivity probes, laser Doppler velocimeters, and other optical techniques.

There are shortcomings in using a tow tank as a flow facility, however. For example, the maximum Reynolds number achievable in the tow tank is lower than that in most wind tunnels. The tank must be sufficiently long to avoid contamination of the flow in the working section by the start/stop and acceleration/deceleration of the models and by the effects of the end walls.

Vortex Generators

The vortex wake was generated by towing a rectangular wing model (NACA 0012) along the axis of the tank. The wing model has a 10.2 cm span and 5.1 cm chord. The maximum dimensions of the wing are dictated by the dimensions of the tow tank and the requirement that the water surface, the tank floor, and the tank walls do not interfere with the vortex phenomena to be investigated. For a tow speed of 40 cm/s, the chord Reynolds number is 2×10^4. According to Sarpkaya and Johnson,[11] who used a delta wing in a tow tank, the depth of submergence h_s is insignificant in the vortex translation in both unstratified and stratifed water for h_s/b_0 greater than about 4.3. They also demonstrated that the dimensionless translation h/b_0 correlates well with the dimensionless time $W_0 t/b_0$, with W_0 changing by a factor of 2. This ensures that W_0 is the appropriate velocity scale for studying the vortex dynamics.

For all of the experiments, therefore, we chose h_s/b_0 to be at least 6.5, with a dimensionless tank depth and half-width of 10.5 and 7.5, respectively. To facilitate the condition $h_s/b_0 > 6.5$, the wing was placed at distances of 1.6 b_0 or 3.2 b_0 above the tank floor. At an angle of attack $\alpha = -10$ deg and tow speed $U_0 = 40$ cm/s, W_0 reduces from 1.1 to 0.8 cm/s as the wing/floor separation reduces from 3.2 to 1.6 b_0. This effectively reduces the equivalent incident angle of the wing. Based on the above findings,[11] the dynamics of the vortex wake are not expected to be modified significantly as long as W_0 is used in forming the dimensionless parameters. One of the main reasons for this is that the core diameter of a trailing vortex at the time of its generation by the towed wing is only 0.1 b_0; also the vortex wake moves away from the tank floor. This is very different from the effect of an insufficient submergence depth because by the time the vortex wake has reached its maximum vertical displacement and is closest to the water surface, the vortex wake has grown to a size of the same order as b_0. Therefore, the preferable compromise for

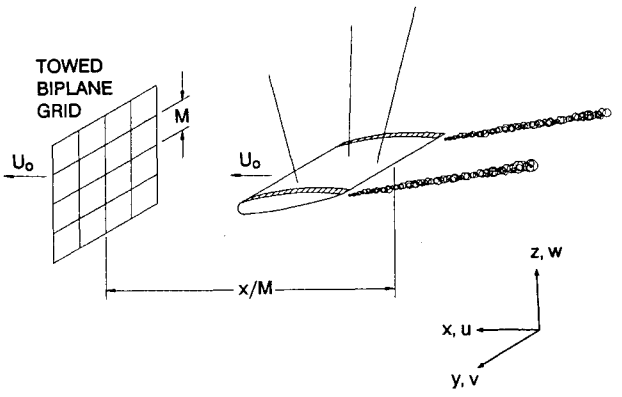

Fig. 2 Sketch of experimental setup in the tow tank.

a finite tank depth is to place the wing close to the tank floor rather than letting the vortex wake move too close to the water surface.

A special mounting technique was used in which the wing is hung upside down on three thin stainless-steel wires (0.008 to 0.013 cm in diameter). This eliminated the strut or sting wake, which can interact with and contaminate the vortex wake during its evolution. The wing model was made of brass so that the weight would be larger than the lift. Thus, the upside-down configuration allows the lift (positive downward) to help stabilize the model (see Fig. 2). To ensure the stability of the mounting system, a shadowgraph was used to image the wing and the suspension wires on a screen. In the working section where the carriage is moving at a constant speed, the wing maintains a steady posture without detectable swinging motion, except when the ambient is extremely turbulent (e.g., within 10 meshes downstream of the medium grid).

Flow Visualization

Fluorescent dye illuminated by various lighting configurations was used to trace the vortex wakes. Just before a run, a thin paste of fluorescent dye (e.g., fluorescein disodium salt) mixed in corn syrup was applied to the two outer edges of the wing. Two dyes of different colors were sometimes used on the two edges to provide a visual distinction between the two trailing vortices. Only a very small amount of dye was needed because the fluorescent dye is highly efficient, especially when illuminated by a UV or argon-ion laser light. During the roll-up of the trailing vortices, the dye that washed away from the wing edges is trapped in the cores and serves as a tracer tracking the two vortices.

From several perspective views (top, end, and side), the motion and evolution of the vortex wake were recorded on 16-mm movie film and in still photographs. For the top view, we recorded the scene through a large mirror (1.2 m wide × 3 m long) mounted above the tank. Banks of UV lights were used to illuminate the vortex wake tracked by the fluorescent dye. The angle of the mirror was adjusted to provide the true top view in accordance with the viewing angle of the cameras. For the end view, visualization was done by illuminating a plane perpendicular to the axis of the tank with a sheet of laser light generated by a laser beam (5-W argon laser by Spectra-Physics) and an oscillating mirror (General Scanning). The cameras were placed at about 30 deg from the tank axis. Corrections were applied to measurements of the vortex trajectories to account for the distortion caused by different viewing angles. For the side view, the vortex wake tracked by the fluorescent dye was illuminated with several banks of UV lights. For all the visual runs, we placed a yardstick inside the tank to record the length scale on film for calibration and correction, if needed, during image analysis and processing.

Ambient Turbulence

Ambient turbulence was generated by towing a grid with square cells (see Fig. 2) through the tank. For a range of integral scales L_f, from small up to a scale comparable to the vortex separation, three different grids were used with meshes of 1.45, 10.2, and 20.3 cm and corresponding solidities of 0.3, 0.2, and 0.1, respectively. The small grid, made of plastic, has elements with cross sections of 0.35 × 0.96 cm^2 with the long side oriented in the streamwise direction. The medium and large grids had square elements with a cross section of 1.27 × 1.27 cm^2; the large grid had the same frame as the medium one with half of the elements removed.

Vortex linking and bursting have vastly different length scales. Intuitively, L_f is expected to be a key parameter governing the type of instability enhanced by ambient turbulence; that is, a small L_f would promote bursting, whereas a large L_f would promote linking. The theoretical prediction of the vortex lifespan due to the onset of linking instability [Eq. (1)] was derived under the assumption that L_f is large compared with the vortex separation. The medium and large grids were selected to generate ambient turbulence with integral scales comparable to or larger than the vortex separation. Such conditions must be met to obtain laboratory results that can be used to verify Eq. (1).

The characteristics of the grid-generated turbulence in terms of turbulence intensity, dissipation rate, and integral scale were measured with an array of four to five quartz-coated hot-film probes (TSI 1248Y) driven by a TSI constant-temperature anemometer (Model 1053B). The probes were mounted on a stainless-steel strut (1.3 cm thick and 15 cm wide), with tapered leading and trailing edges, and towed behind the grid at the same speed as the grid. Three of the probes were oriented to measure the longitudinal (U) and vertical (W) velocity components, and at least one probe was rotated 90 deg to measure the longitudinal and lateral velocity components. The hot-film probes were calibrated by towing them (with no grid) at several speeds in a quiescent fluid. The tow speeds and the corresponding voltage outputs of the two film elements were fitted with second-degree polynomials. The two velocity components were derived from the outputs of the two elements using the cosine law.

The signals were low-pass filtered at 500 Hz at a sampling rate of 1 kHz. Depending on the distance downstream of the grid in terms of the mesh size x/M, we selected from each run about 8 to 20 s of data in which the time series was observed to be stationary. This corresponds to the portion of the time series recorded in the working section, i.e., data unaffected by start/acceleration and stop/deceleration of the grid, by the probe array, and by tank-wall reflection. It was discovered that these transient motions set up a relatively low-amplitude (≈0.02 U) and long-wavelength (≈6 m) seiche motion in the tank that becomes apparent at large x/M where the turbulence intensity is weak. To reduce the contamination of the seiche motion, we adopted a running mean algorithm by dividing the time series into blocks of 500 data points and ensemble-averaging the local statistical parameters over these blocks. The algorithm is effectively a high-pass filter that significantly attenuates the kinetic energy of the seiche motion but not that of the energy-containing turbulent fluctuations.

The ambient water usually returns to a quiescent state in about 1.5 h after a run. We consider the ambient to be quiescent when the maximum residue motion in the tank is less than 0.08 cm/s. The motion in the tank is monitored by tracking purple streaks left behind fine potassium permanganate crystals released into the water column. For a reference run without the grid, we wait until the tank is indeed quiescent.

Vibration of the tow system introduces noise in the hot-film data that limits the minimum turbulence intensity and dissipation that can be measured by the probes. This noise is not the same as the background turbulence that is measured in a wind tunnel. To estimate the system noise level, we conducted tests by towing the probes in a quiescent fluid. The noise levels, defined by the rms of the velocity components divided by the tow speed and estimated from the results of the noise tests, were found to be 0.3, 0.13, and 0.08% for the u, v, and w components. Consequently, we removed the noise

from the signals by subtracting the mean square noise from the mean square signals.

From the experimental data, we can estimate the dissipation rate according to the formula derived for locally isotropic turbulence[18]:

$$\varepsilon = 15\nu\overline{(\partial u/\partial x)^2} \tag{4a}$$

or

$$\varepsilon = 15\nu\overline{(\partial u/\partial t)^2}/\bar{U}^2 \tag{4b}$$

using Taylor's hypothesis, where ν is the kinematic viscosity. Therefore, we can estimate the dissipation rate from the mean square of the time derivatives of the longitudinal turbulence velocity fluctuations, with the noise subtracted similar to that for the mean square velocity components. By towing the wing at different distances behind the grid, we were able to study the vortex wake in a turbulent environment with a range of integral scales and turbulence intensities to determine the effects of the ambient turbulence on its evolution (see Fig. 2). Note that the grid turbulence varies with time after the tow or with distance behind the grid. For example, the turbulence intensity varies as $t^{-0.65}$ or $x^{-0.65}$ in a homogeneous fluid.[19]

IV. Results

Ambient Turbulence Results

Hot-film measurements were made to characterize the ambient turbulence generated by the three grids. From the time series of the velocity components, we derived the turbulence intensity, the dissipation rate, and the integral scale. Dimensionless parameters were formed by using M or b_0 and U or W_0 as the length and velocity scales, respectively.

Figures 3 through 5 show the decay of the mean square of the components of the turbulence kinetic energy ($\overline{u^2}/\bar{U}^2$, $\overline{v^2}/\bar{U}^2$, and $\overline{w^2}/\bar{U}^2$), with the mean square noise subtracted, as a function of x/M or x/b_0 for the three grids. The typical scatter of the data ($\pm$ one standard deviation) is represented by error bars. In general, the grid turbulence generated in the tow tank is not very isotropic. The ratios of $\overline{w^2}/\overline{u^2}$ are about 0.4, 0.6, and 0.6 for the small, medium, and large grids, respectively, with the ratio of $\overline{v^2}/\overline{w^2} \simeq 1$. The lines fairing through most of the data points show a slope of $(x/M)^{-1.3}$ or $(x/b_0)^{-1.3}$, which is consistent with wind tunnel measurements.[19] At large $x/M > 200$, where the signal-to-noise ratio is relatively low, the data do not necessarily follow the

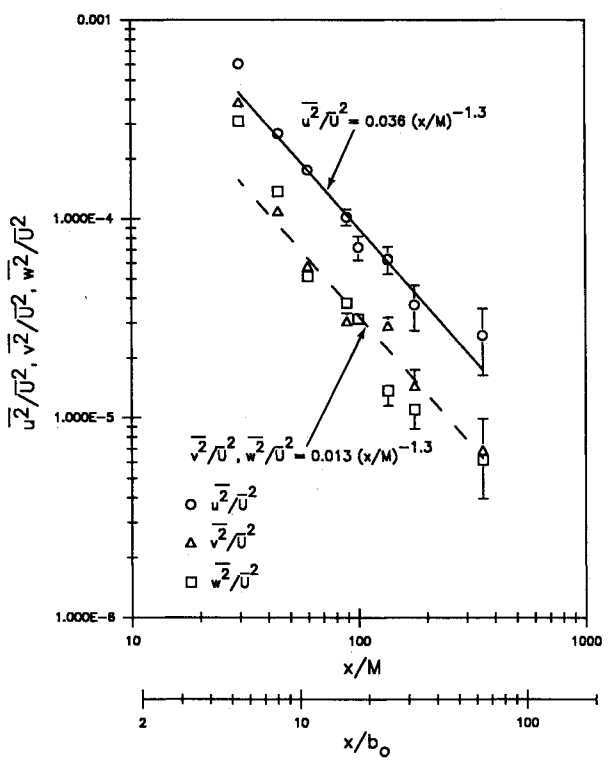

Fig. 3 Decay of components of turbulence kinetic energy in grid turbulence, M = 1.45 cm.

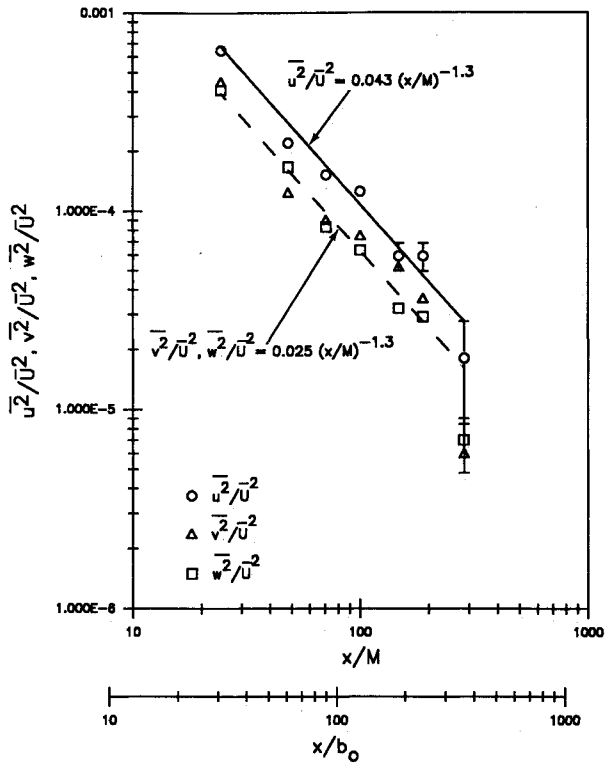

Fig. 4 Decay of components of turbulence kinetic energy in grid turbulence, M = 10.2 cm.

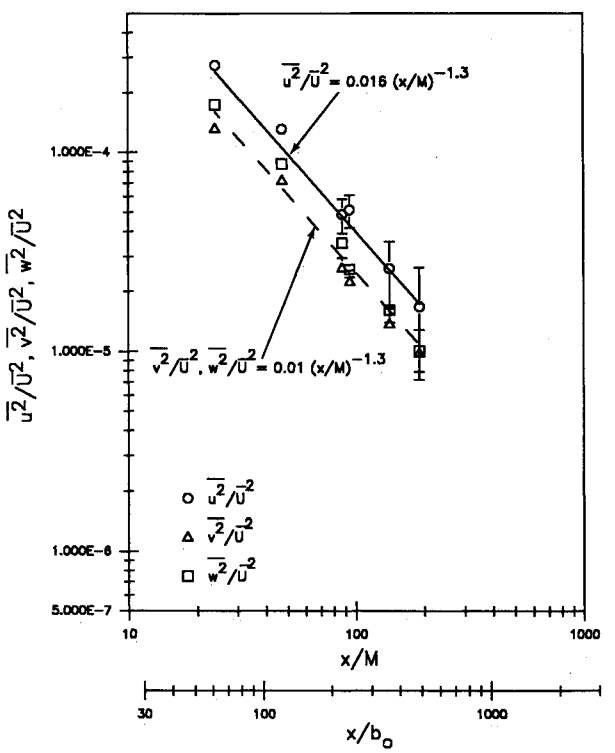

Fig. 5 Decay of components of turbulence kinetic energy in grid turbulence, M = 20.3 cm.

$(x/M)^{-1.3}$ trend. Also, the data at large x/M are contaminated by a seiche motion set up by the starting/stopping and acceleration/deceleration of the grid.[20]

The total turbulence energy for the three grids, $q^2/2\bar{U}^2$, can be obtained by summing up the mean square of the corresponding components, i.e., $q^2 = (\overline{u^2} + \overline{v^2} + \overline{w^2})/2$. Figure 6 shows the decay of the total turbulence energy for the three grids. As expected, they all follow $(x/M)^{-1.3}$ or $(x/b_0)^{-1.3}$, just as their individual components do. The data for the medium and large grids collapse onto a single curve in the x/b_0 coordinate. For the small grid, the value of $q^2/2\bar{U}^2$ at $x/M = 30$ or $x/b_0 = 5.44$ is considerably higher than if the trend were extended from its larger x/b_0 counterparts. This is because the corresponding distance $x = 43.5$ cm is simply too close to the grid, and the turbulence field has not relaxed to an equilibrium state.

Figure 7 shows the decay of the dimensionless dissipation rate ε^* derived from the time series of the longitudinal velocity components. Here the noise is subtracted from the signals. For the three grids, the dissipation rates follow $(x/b_0)^{-0.77}$, as indicated by the straight lines fairing through the individual data sets. The lines may be represented by

$$\varepsilon^* = 9.07(x/b_0)^{-0.77} \quad \text{for} \quad M = 1.45 \text{ cm} \tag{5a}$$

$$\varepsilon^* = 28.2(x/b_0)^{-0.77} \quad \text{for} \quad M = 10.2 \text{ and } 20.3 \text{ cm} \tag{5b}$$

The previous equations were used to design the experiments for investigating the effects of ambient turbulence on the vortex instability. For large distances $x/M > 200$, at which the signal-to-noise ratio is too low to provide meaningful measurements, the dissipation rates were extrapolated according to these equations.

The integral scale of the ambient turbulence L_f generated by the three grids is estimated from the integration of the autocorrelation coefficient of the longitudinal velocity component[18] and is presented in Fig. 8. The trend of increasing L_f/b_0 with the increase in x/b_0 is established. The results show that the L_f generated by the small grid is small compared with b_0, whereas that generated by the medium and large grids is about the same as or larger than b_0. For instance, L_f/b_0 for the medium grid as a function of x/b_0 may be approximated by

$$L_f/b_0 = 0.0028(x/b_0) + 0.357 \tag{6}$$

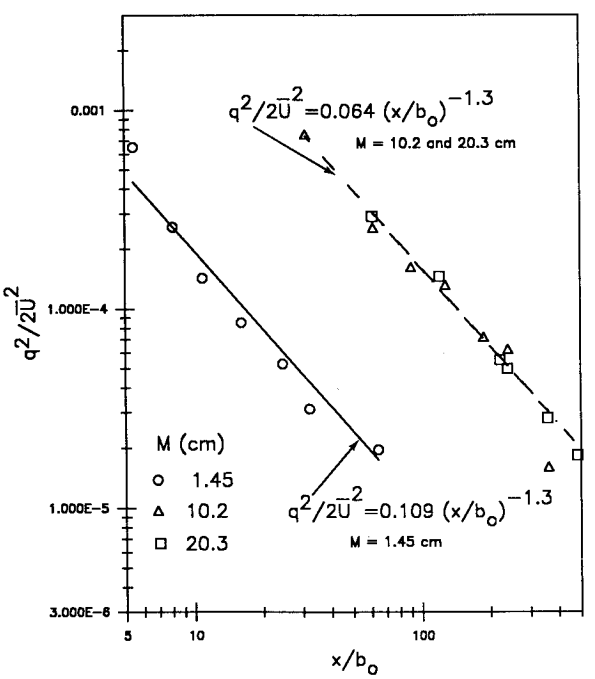

Fig. 6 Decay of total turbulence kinetic energy in grid turbulence.

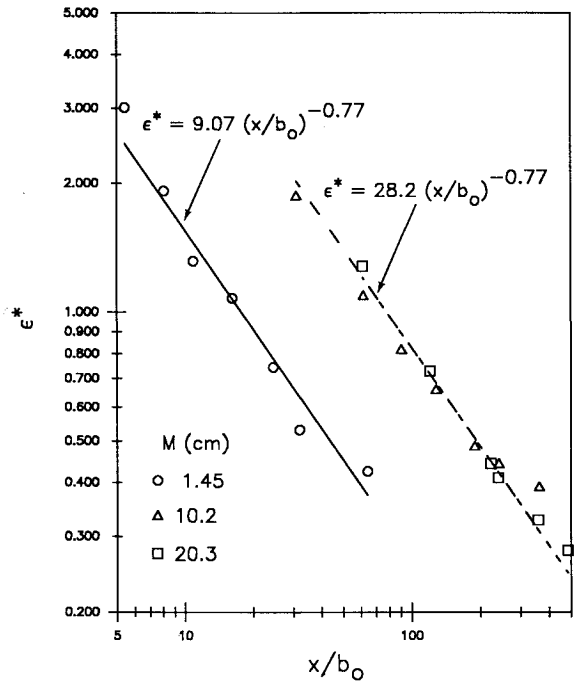

Fig. 7 Decay of dissipation rate in grid turbulence.

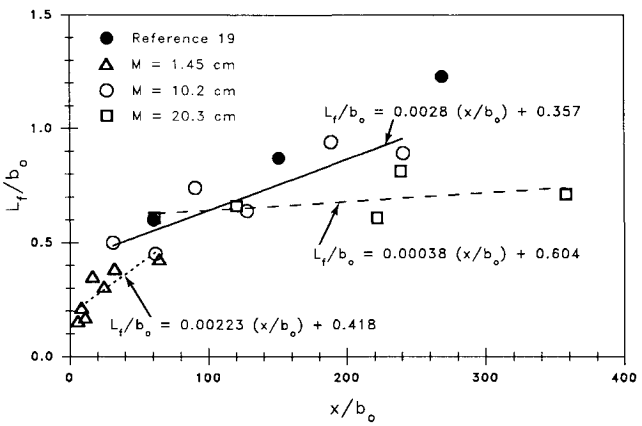

Fig. 8 Measurements of integral scale in grid turbulence.

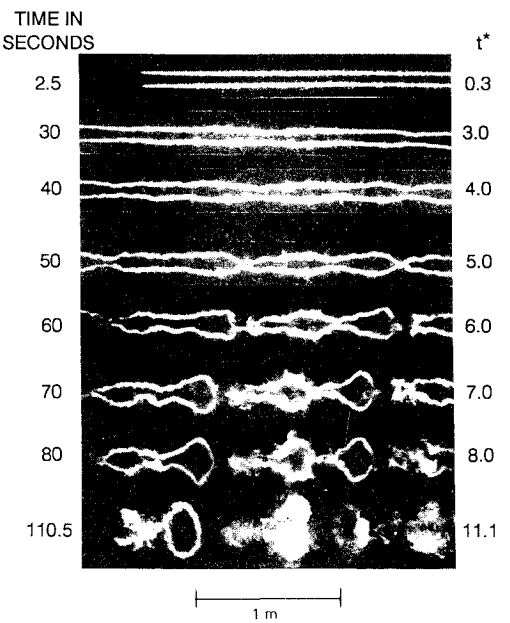

Fig. 9 Development of a linking instability in a quiescent, neutrally stable environment.

For large distances downstream of the grid (i.e., $x/M > 200$), L_f is at least as large as b_0.

From the equations for the total turbulence kinetic energy (Fig. 6), the dissipation rate [Eq. (5)], and the integral scale [Eq. (6)], we can verify whether Eq. (3) is valid for anisotropic turbulence. For turbulence generated by the medium grid and at large x/b_0, we find that

$$\varepsilon = 0.18q^2/L_f \tag{7}$$

which is in the same form as Eq. (3) except that the constant is different. Apparently, the role of anisotropy is to reduce the constant term from 0.25 to 0.18. The previous equation is a convenient alternative for estimating the dissipation rate, provided q^2 and L_f are available.

Visualization Results

Visual experiments were conducted to determine the effects of weak ambient turbulence in reducing the lifespan of a vortex wake. Several reference runs were made first by towing the NACA wing in the quiescent tank. Figure 9 is a top view of a trailing vortex wake at several time intervals after its generation. Initially, the trailing vortex pair manifests itself as two parallel straight lines representing the thin cores. The straightness of the cores is an indication of the excellent stability of the tow/suspension system, because any lateral swing of the wing would cause deterioration in the straight path of the cores. It is evident in this figure that vortex linking is the sole mode of instability. The first linking is observed at $t^*_f \approx 5$. The wavelengths of the linking range from 5 b_0 to 9 b_0. The linking may best be described as a deterministic process superposed with a certain degree of randomness, where randomness refers to the discrete locations at which linking takes place. Here, the coherent vortex motion disappears soon after the linking occurs; at others, the coherent vortex may persist for quite some time.

As measured from the movie records, the first and subsequent linkings are observed between $t^*_f \approx 4.3$ to 6.6. The vortex separation is about the same as the span ($S = 10.2$ cm) at the trailing edge but quickly decreases to about 8 cm, which is consistent with lifting line theory, i.e., $b_0 = \pi S/4$. At $t^* = 6$, the relative vortex strength, as measured from the ratio of the translation speed, is about 60% of its initial value.

Figure 10 shows a top view of a trailing vortex wake in the presence of ambient turbulence generated by the large grid at $x/b_0 = 355$ ($\varepsilon^* \approx 0.2$). Linking is still the predominant mode of vortex instability, with only a few bursting events observed before and during linking. There are considerable spatial and temporal variations in the linking process. For the same time after passage of the wing, the two vortex trails show more distortion and diffusion than their nonturbulent counterparts (Fig. 9). As a result, linkings are observed between $t^*_f \approx 2$ and 4, depending on where the linking occurs. The dominant wavelength of the linking taking place in the middle of the area shown in the figure does not differ much from that of the reference case. These visual results have demonstrated that the lifespan decreases with decreasing x/b_0, as anticipated. Here, the lifespan has been generalized to include the time at which local bursting takes place, which is not modeled in Eq. (1).

Figure 11 is a close-up view of the development of a vortex wake that is exposed to relatively stronger ambient turbulence ($\varepsilon^* \approx 0.4$) than that shown in Fig. 10 using the same large grid. It can clearly be seen that both linking and bursting take

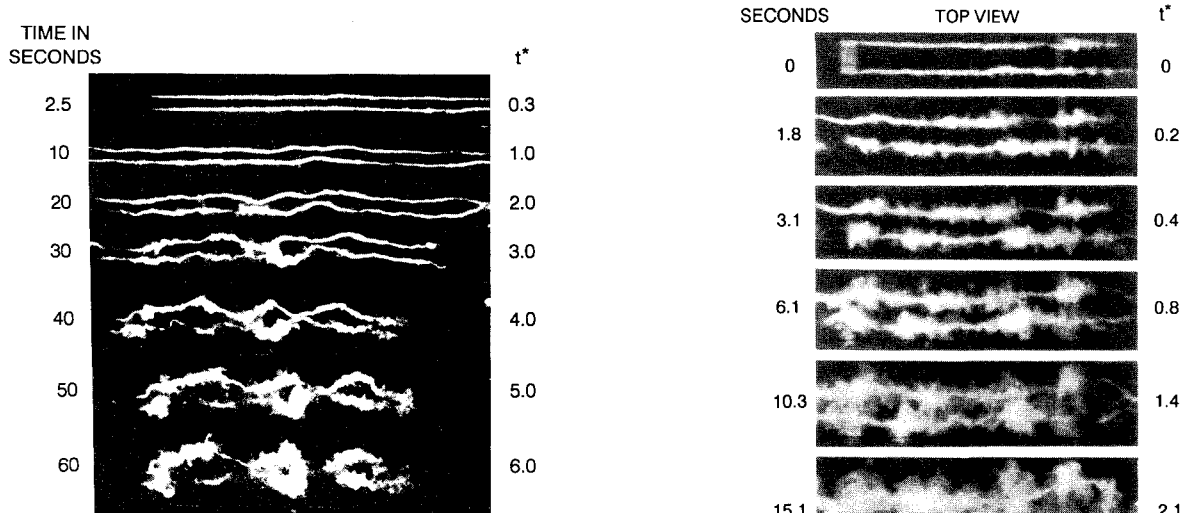

Fig. 10 Evolution of a trailing vortex wake in grid turbulence.

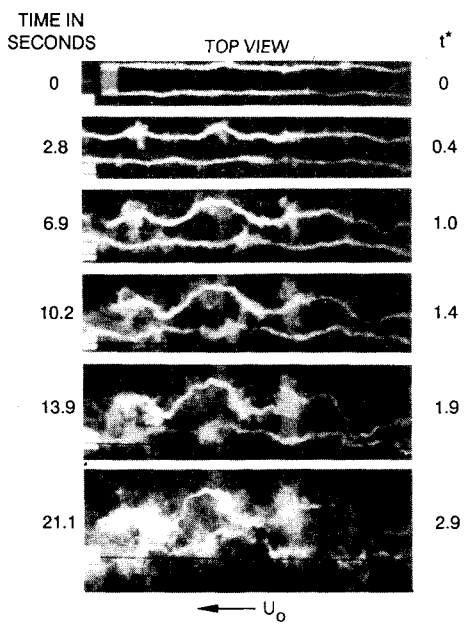

Fig. 11 Simultaneous development of vortex linking and bursting in grid turbulence.

Fig. 12 Bursting shown as the dominant mode of vortex instability in grid turbulence.

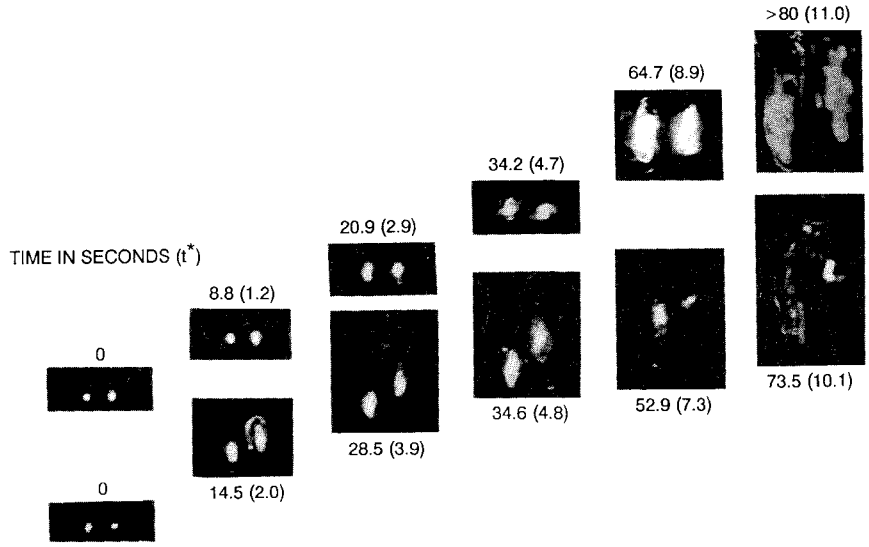

Fig. 13 End views of two trailing vortex pairs illuminated with a sheet of laser light.

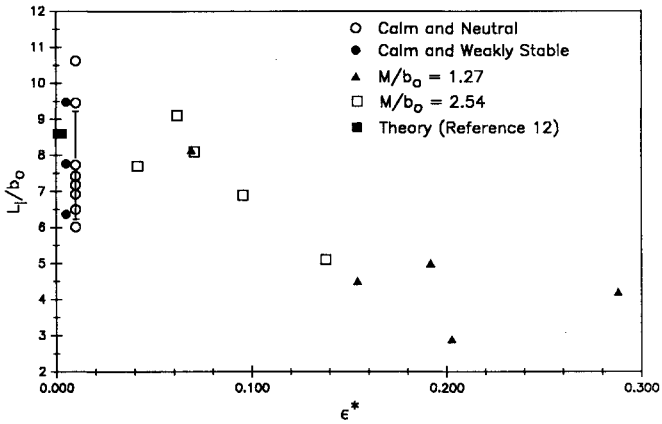

Fig. 14 Variations of the dominant wavelength of vortex linking with the dissipation rate.

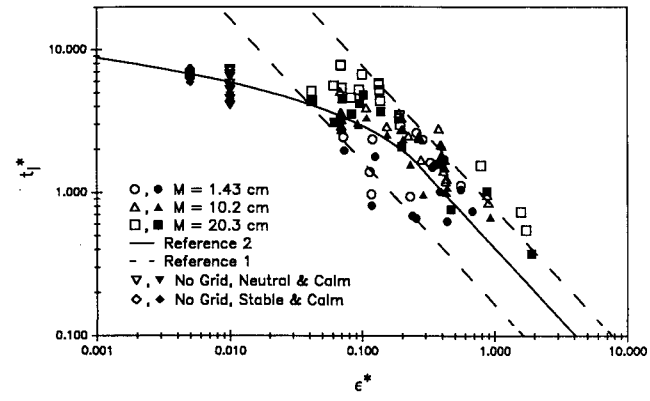

Fig. 15 Lifespan of a trailing vortex wake as a function of the dissipation rate.

place in relatively strong ambient turbulence. The dominant wavelength of the linking is about three times the vortex separation, which is considerably shorter than that in a quiescent ambient (see Fig. 1 or 10). With further increase in the turbulence intensity ($\varepsilon^* \approx 0.5$), bursting becomes the dominant mode that destroys the vortex wake, as observed in Fig. 12. There is no sign of any linking development in the short duration before the vortex wake is completely destroyed by bursting.

Figure 13 shows the end views of two vortex wakes in quiescent and turbulent ambients ($M = 20.3$ cm and $\varepsilon^* \approx 0.1$). There are definite differences in the coherency, symmetry, and integrity of the vortices for the two cases at comparable times. Mixing induced by the ambient turbulence increases the diffusion of the vortex cores and introduces asymmetry (e.g., relative displacement) in the recirculation cells.

Careful examination of the visual results has led to the identification of several trends. In the wake of the medium and large grids, the onset of instability is predominantly of the linking type for small ε^* but shifts to the bursting type as ε^* increases. In the wake of the small grid, the induced instability is of the bursting type. Quantification of these trends is given later in Sec. IV. It is important to point out that vortex instability is an extremely localized phenomenon, as is evident from the visual results. The vortex motion is highly organized and potentially hazardous to followers except at discrete locations at which the first and subsequent linking or bursting events take place. This must be kept in mind when optimizing aircraft spacing using laboratory and field results.

From the visual records, we measured the dominant wavelength of vortex linking L_ℓ in the wakes of the medium and large grids. The dimensionless wavelength L_ℓ/b_0 is plotted in Fig. 14 against ε^*. Also shown are the theoretical prediction of Crow[12] ($L_\ell/b_0 = 8.6$) and measurements in calm (neutral and weakly stable) ambient conditions. The trend of inverse proportionality of L_ℓ/b_0 with ε^* is clearly established. Note the ε is proportional to q^2/L_f [Eq. (7)]. The aforementioned trend indicates that L_ℓ/b_0 decreases with $q^2/\bar{U}^2$ and $(L_f/b_0)^{-1}$, which is consistent with the visual observations.

Effects of Dissipation Rate on Lifespan

The visualization results were used to derive the lifespan of the vortex wake as a function of the dissipation rate. Attempts were made to verify the theory developed by Crow and Bate[2] [Eq. (1)], which has been subjected to limited verification via field experiments.[1] For consistency, we define the lifespan to be the time at which linking or bursting is observed from the visual records (top view). To account for the decaying turbulence field, the dissipation rate is defined as the average of the dissipation rates measured at the time of vortex generation and at the time of the linking or bursting.

In Fig. 15, we plot the dimensionless lifespan $t_\ell^* = W_0 t_\ell^*/b_0$ vs the dimensionless dissipation rate $\varepsilon^* = (\varepsilon b_0/W_0^3)^{1.3}$. The solid and dashed curves correspond to the theory of Crow and Bate[2] [Eq. (1)] and to the envelope of Tombach's field data[1] [Eq. (2)]. The various symbols represent our laboratory results derived from the visual records (see legend). The solid and open symbols represent, respectively, the lifespans at which the first linking or bursting event and subsequent events take place. In a few cases when the ambient turbulence is weak ($\varepsilon^* < 0.08$), four or more sub-

sequent linking events may be observed before the vortex wake loses its coherent appearance. Note that Eq. (1) predicts the lifespan of the first linking.

Also included in Fig. 15 are the results in a quiescent environment under neutral and weakly stable conditions. For the stable cases, the water in the tank was thermally stratified with a Brunt-Vaisala frequency less than 0.02 rad/s. The corresponding stratification parameter, defined as the product of the Brunt-Vaisala frequency and the wing span,[6] is less than 0.2. Under these conditions, the dissipation rate was too small to be measured with the hot-film probes. We estimated the dissipation rate under the assumption that the residue motion (<0.08 cm/s) in the tank is sinusoidal or cellular with a wavelength of twice the tank width or 2.4 m. According to Eq. (4), the maximum value of ε^* is estimated to be 0.007, i.e., of the order of 0.01. For the weakly stable cases, ambient turbulence is suppressed, which is particularly true in the atmosphere where zero turbulence is improbable under neutrally stable conditions. On the other hand, the effect of such a weak stratification on the vortex wake is small.[6] Therefore, we assume ε^* for the weakly stable cases to be half of that for the neutrally stable cases, or 0.005. In the nearly quiescent environment, Eq. (1) (solid curve) predicts only small changes of t_f^* with ε^*, and errors resulting from an inaccurate estimate of ε^* are relatively small. For the runs under quiescent ambient conditions, the average lifespan of the first linking (solid symbols) is comparable in a weakly stable and in a neutral environment. In the atmosphere, it is likely that the lifespan in the former may be longer than in the latter provided that the effect of turbulence suppression overwhelms that of stratification.

The large data spread in Fig. 15 is to be expected due to the random nature of the linking and bursting processes and the broad inclusion of several data types. We have attempted to reduce the data scatter by dividing them into subgroups of similar types. For a fair comparison, it is appropriate to consider the lifespan due to linking alone, as illustrated in Fig. 16. The removal of lifespan data due to bursting in this figure definitely reduces the data spread, particularly when we consider only the solid symbols, which represent the lifespan due to the first linking as the theory predicts.

From the visual results, a definite trend is the absence of vortex linking for the runs with the small grid. For further observation, we present in Fig. 17 the laboratory results of the lifespan due to vortex bursting alone, which do not agree well with those predicted by Eq. (1). Due to the sporadic nature of vortex bursting, it is not surprising that considerable data scatter is observed. However, several interesting trends can be extracted from the results. We will first focus on the runs with the small grid (circles). It is evident that bursting is the dominant mode of vortex instability induced by ambient turbulence with an integral scale much smaller than the vortex separation for ε^* as low as 0.072. For relatively small ε^*, where bursting is observed only for these runs, the lifespan due to the first bursting is considerably below the solid curve,

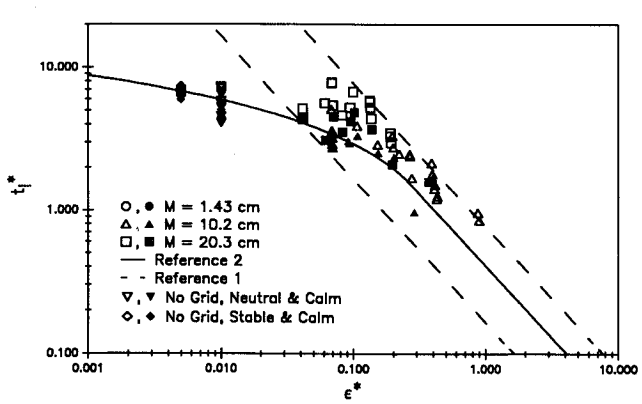

Fig. 16 Lifespan of a trailing vortex wake due to vortex linking as a function of the dissipation rate.

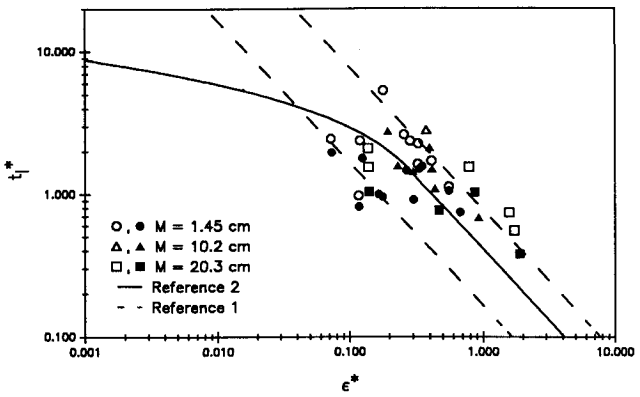

Fig. 17 Lifespan of a trailing vortex wake due to vortex bursting as a function of the dissipation rate.

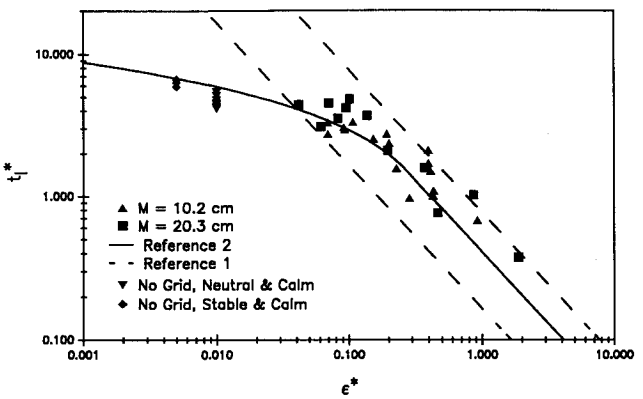

Fig. 18 Lifespan of a trailing vortex wake as a function of the dissipation rate with the results of the small grid excluded.

i.e., Eq. (1). Note that Eq. (1) was derived for linking instability under the assumption that the integral scale is large compared with the vortex separation. As ε^* increases, the deviation between the laboratory results and the predictions decreases. In other words, small-scale turbulence is very effective in promoting vortex instability in the form of vortex bursting, at least at low Reynolds numbers. For example, at ε^* between 0.1 and 0.3, the lifespan may be three to four times shorter than the predicted value. In reality, turbulence with an integral scale much smaller than that of the vortex separation seldom occurs, except perhaps very near the ground.

For the runs with the medium and large grids, the first vortex bursting is observed for $\varepsilon^* > 0.19$ and 0.4, respectively. However, linking and bursting are by no means mutually exclusive events, as illustrated in Fig. 11.

Based on the previous discussion, it is clear that we should only include the results of the medium and large grids when verifying Eq. (1). Indeed, when we exclude the results of the small grid and include the lifespan of the first linking or bursting, the data scatter is greatly reduced (see Fig. 18) from that originally observed in Fig. 15. There is a reasonable correlation between the predicted and the laboratory-measured lifespans for a range of ε^* almost two decades wider than that of the field experiments.[1] For such a wide range of ε^*, the mode of vortex instability shifts from linking to bursting as ε^* increases. Thus, the lifespan due to both linking and bursting depends solely on the single dimensionless parameter $\varepsilon^* = (\varepsilon b_0/W_0^3)^{1/3}$. Here, we have extended the application of Eq. (1) to include both linking and bursting instability, at least for turbulence with large integral scales as compared to the vortex separation.

Except for runs under quiescent ambient conditions, most of the data points are above the solid curve, which is consistent with the trend seen in the field experiments.[1] This indicates that Eq. (1) tends to underpredict the lifespan of the vortex wake in a turbulent environment. For practical applications, one must keep in mind that vortex linking and bursting are

localized phenomena, particularly at their onset. Except at discrete places where linking or bursting takes place, the vortex motion is largely coherent, and the potential hazard remains even after the onset of vortex instability (see Figs. 10 and 11).

V. Summary and Recommendations

Tow tank experiments were conducted to simulate the effects of atmospheric turbulence on the evolution of vortex wakes. Turbulence was generated by towing one of three grids (M = 1.45, 10.2, and 20.3 cm) upstream of an NACA 0012 wing (b_0 = 8.0 cm). The ambient turbulence in terms of turbulence intensity and dissipation rate was derived from hot-film data. The evolution of the vortex wake in the grid turbulence field was observed. The lifespan of the vortex wake, defined as the time at which linking or bursting takes place, is a function of the dissipation rate and the integral scale of the ambient turbulence.

1) In a quiescent environment ($\varepsilon^* < 0.01$), linking is the dominant mode of vortex instability. The average dominant wavelength was measured to be about 7.8 b_0 as compared with the theoretical value of 8.6 b_0.

2) Ambient turbulence with integral scales comparable to or larger than the vortex separation promotes linking instability; both the lifespan of the vortex wake and the dominant wavelength of the linking instability are shortened. As the dimensionless dissipation rate increases ($\varepsilon^* < 0.2$), vortex bursting emerges at various places along the sinuously distorted vortex wake. In strong turbulence ($\varepsilon^* > 0.4$), vortex bursting becomes the dominant mode of vortex instability.

3) Turbulence generated by the small grid, which has integral scales smaller than the vortex separation, promotes predominantly vortex bursting. For relatively weak turbulence (ε^* as low as 0.072), the lifespan is much shorter (by as much as a factor of 4) than that due to linking/bursting induced by turbulence generated with the medium and large grids.

4) With the exclusion of the results of the small grid, the laboratory measurements compare reasonably well with the theory[2] and with field measurements,[1] especially when the lifespan of the first link or burst is used in the comparison. For practical consideration, our results have confirmed that t_v^* depends solely on ε^* for both linking and bursting instabilities. We must emphasize that vortex instability is an extremely localized phenomenon; the vortex motion is highly coherent except at discrete points of the first or subsequent vortex linking or bursting events. Most of the laboratory data (except those obtained in a quiescent environment) are above the theoretical prediction, which is consistent with the trend of the field results. With due consideration of the aforementioned trend and of the localized nature of the onset of vortex instability, we recommend the adaptation of an equation for the dimensionless separation time between takeoffs and/or landings for small followers by multiplying Eq. (1) by a safety factor of 2. For large followers, the safety factor may be adjusted according to their classes.

Acknowledgments

This study was sponsored by the Transportation Systems Center, U.S. Department of Transportation, under SBIR Contract DTRS-57-87-C-00109, and by an IR & D fund from QUEST. The author would like to thank R. A. Srnsky for carrying out the tow tank experiments.

References

[1]Tombach, I., "Observations of Atmospheric Effects of Vortex Wake Behavior," *Journal of Aircraft*, Vol. 10, No. 11, 1973, pp. 641–647.

[2]Crow, S. C., and Bate, E. R., Jr., "Lifespan of Trailing Vortices in a Turbulent Atmosphere," *Journal of Aircraft*, Vol. 13, No. 7, 1976, pp. 476–482.

[3]Bilanin, A. J., Teske, M. E., and Hirsh, J. E., "Neutral Atmospheric Effects on the Dissipation of Aircraft Vortex Wakes," *AIAA Journal*, Vol. 16, No. 9, 1978, pp. 956–961.

[4]Saffman, P. G., "The Motion of a Vortex Pair in a Stratified Atmosphere," *Studies in Applied Mathematics*, Vol. LI, No. 2, 1972, pp. 107–119.

[5]Hirsh, R. S., "A Numerical Simulation of Vortex Motion in a Stratified Environment and Comparison with Experiments," *Johns Hopkins APL Technical Digest*, Vol. 6, No. 3, 1985, pp. 203–210.

[6]Greene, G. C., "An Approximate Model of Vortex Decay in the Atmosphere," *Journal of Aircraft*, Vol. 23, No. 7, 1986, pp. 566–573.

[7]Olsen, J. H., "Results of Trailing Vortex Studies in a Towing Tank," *Aircraft Wake Turbulence and Its Detection*, edited by J. H. Olsen, A. Goldburg, and M. Rogers, Plenum Press, New York, 1971, pp. 455–472.

[8]Kirkman, K. L., Brown, C. D., and Goodman, A., "Evaluation of Effectiveness of Various Devices for Attenuation of Trailing Vortices Based on Model Tests in a Large Towing Basin," NASA CR-2202, Dec. 1973.

[9]Lezius, D. K., "Study of the Far Wake Vortex Field Generated by a Rectangular Airfoil in a Water Tank," National Aeronautics and Space Administration, NASA-TM-X-62274, May 1973.

[10]Sarpkaya, T., "Trailing Vortices in Homogeneous and Density-Stratified Media," *Journal of Fluid Mechanics*, Vol. 136, Nov. 1983, pp. 65–109.

[11]Sarpkaya, T., and Johnson, S. K., "Trailing Vortices in Stratified Fluids," Naval Postgraduate School, Rept. NPS-69-82-003, Monterey, CA, 1982.

[12]Crow, S. C., "Stability Theory for a Pair of Trailing Vortices," AIAA Paper 70-53, Jan. 1970.

[13]Hall, M. G., "Vortex Breakdown," *Annual Review of Fluid Mechanics*, Vol. 4, 1972, pp. 195–218.

[14]Bilanin, A. J., and Widnall, S. E., "Aircraft Wake Dissipation by Sinusoidal Instability and Vortex Breakdown," AIAA Paper 73-107, Jan. 1973.

[15]Widnall, S. E., Bliss, D. B., and Zalay, A., "Theoretical and Experimental Study of the Stability of a Vortex Pair," *Aircraft Wake Turbulence and Its Detection*, edited by J. H. Olsen, A. Goldburg, and M. Rogers, Plenum Press, New York, 1971, pp. 305–329.

[16]Leibovich, S., "The Structure of Vortex Breakdown," *Annual Review of Fluid Mechanics*, Vol. 10, 1978, pp. 221–246.

[17]Batchelor, G. K., *The Theory of Homogeneous Turbulence*, Cambridge Univ. Press, Cambridge, UK, 1953.

[18]Hinze, J. O., *Turbulence*, McGraw-Hill, New York, 1959.

[19]Comte-Bellot, G., and Corrsin, S., "Simple Eulerian Time Correlation of Full- and Narrow-Band Velocity Signals in Grid-Generated, 'Isotropic' Turbulence," *Journal of Fluid Mechanics*, Vol. 48, Part 2, 1971, pp. 273–337.

[20]Lange, R. E., "Decay of Turbulence in Stratified Salt Water," Ph.D. Dissertation, Scripps Institution of Oceanography, 1974.